

Recent results from the BRAHMS experiment

P. Staszela^a (for the BRAHMS* Collaboration)

^aJagiellonian University, Institute of Physics,
ul. Reymonta 4, 30-059 Kraków, Poland

We present recent results obtained by the BRAHMS experiment at the Relativistic Heavy Ion Collider (RHIC) for the systems of Au+Au and Cu+Cu at $\sqrt{s_{NN}} = 200$ GeV and at 62.4 GeV, and p+p at $\sqrt{s_{NN}} = 200$ GeV. BRAHMS explores reaction dynamics and properties of the hot and high energy density matter produced in ultra-relativistic heavy-ion collisions versus its longitudinal expansion. Overall charged-particle production and particle spectra over a large rapidity interval and p_T range are presented. Nuclear modification factors for Au+Au and Cu+Cu collisions are discussed. The observed number of charged particles produced per unit of rapidity in the central rapidity region indicates that a high energy density system is produced at the initial stage of the Au+Au reaction. Analysis of anti-particle to particle ratios as a function of rapidity and collision energy reveal that particle populations at the chemical freeze-out stage for heavy-ion reactions at and above SPS energies are controlled by the baryon chemical potential. From the particle spectra we deduce significant radial expansion ($\beta \approx 0.75$), as expected for systems created with a large initial energy density. We also measure the elliptic flow parameter v_2 versus rapidity and p_T . A weak dependence on rapidity of the p_T differential v_2 is observed. We present rapidity dependent p/π ratios within $0 < y < 3$ for Au+Au and Cu+Cu at $\sqrt{s_{NN}} = 200$ GeV. The ratios are enhanced in nucleus-nucleus collisions as compared to p+p collisions. The particle ratios are discussed in terms of their system size and rapidity dependence. We compare R_{AA} for Au+Au at $\sqrt{s_{NN}} = 200$ GeV and at 62.4 GeV, and for Au+Au and Cu+Cu at $\sqrt{s_{NN}} = 62.4$ GeV. R_{AA} is found to increase with decreasing collision energy, decreasing system size, and when going towards more peripheral collisions. However, R_{AA} shows only a very weak dependence on rapidity (for $0 < y < 3.2$), both for pions and protons.

1. INTRODUCTION

Reactions between heavy nuclei provide a unique opportunity to produce and study nuclear (hadronic) matter far from its ground state, at high densities and temperatures. From the onset of the formulation of the quark model and the first understanding of the nature of the binding and confining potential between quarks about 30 years ago, it has been realized that at very high density and temperature, hadronic matter may undergo a transition to a more primordial form of matter. This proposed state of matter named the quark gluon plasma (QGP) [1], is characterized by a strongly reduced interaction

*For the full list of BRAHMS and acknowledgments see appendix 'Collaborations' of this volume

among its constituents, quarks and gluons, such that the partons would exist in a nearly free state [2]. Experimental attempts to create the QGP in the laboratory by colliding heavy nuclei have been carried out for more than 20 years. During this period, center of mass energies per pair of colliding nucleons have risen steadily from the $\sqrt{s_{NN}} = 1$ GeV domain of the Bevalac at LBNL, to energies of $\sqrt{s_{NN}} = 5$ GeV at the AGS at BNL, and to $\sqrt{s_{NN}} = 17$ GeV at the SPS at CERN. Although a number of signals suggesting the formation of a very dense state of matter have been observed, no solid evidence for QGP formation was found at these lower energies.

In mid-August 2001 systematic data collecting by the four RHIC experiments, namely BRAHMS [3], PHENIX [4], PHOBOS [5] and STAR [6], began at the energy of $\sqrt{s_{NN}} = 200$ GeV. The RHIC operations started a new era of studies of ultra-relativistic nucleus-nucleus collisions. One of the main results obtained up to the present at RHIC is the observation of significant elliptic flow in central Au+Au collisions. The large flow signal, one that is consistent with the hydrodynamic evolution of a perfect fluid [7–10], indicates a strongly interacting QGP, contrary to initial expectations. Also observed is strong jet suppression [11], which is predicted within the Quantum Chromo-Dynamics theory (QCD) as a consequence of the creation of a dense colored medium [12]. This last observation was supplemented by d+Au measurements showing the absence of suppression, but rather a Cronin type enhancement at the central rapidity region, thus excluding an alternative interpretation of the suppression in terms of initial state parton saturation (CGC) effects. Another measurement that strongly supported the scenario of jet quenching was the disappearance of the away-side jet [13,14] in central Au+Au collisions, whereas for d+Au and peripheral Au+Au near side and away side back-to-back jet correlations have been measured. Its large rapidity range and p_T coverage allows BRAHMS to study the properties of the produced medium as a function of its longitudinal expansion. The measurement of rapidity evolution of the nuclear modification factor for d+Au performed by BRAHMS shows that at more forward rapidities the hadronic yields are suppressed as compared to scaled p+p interactions [15]. The suppression was even stronger for central collisions. Both observations can be quantitatively described within the framework of the CGC [12,16].

2. BRAHMS DETECTOR SETUP

The BRAHMS (Broad Range Hadron Magnetic Spectrometers) [17], experimental setup consists of a set of global detectors and two spectrometer arms: a Mid-Rapidity Spectrometer (MRS) that operates in the polar angle range from 30 to 90 degrees, and a Forward Spectrometer (FS) that operates in the range between 2.3 and 30 degrees. Global detectors are used to measure the global features of the collision such as the overall particle multiplicity and collision centrality, position of the collision vertex and, more recently, information on the reaction plane orientation which can be used for azimuthal flow analysis. For the momentum measurements in the MRS we use two tracking devices and one dipole magnet. Particle identification (PID) is done by Time-of-Flight (TOF) measurement and by using threshold Cherenkov detector C4. In the FS two Time Projection Chambers (TPC) and three Drift Chambers (DC) deliver particle track segments to allow excellent momentum resolution using three dipole magnets. PID in the FS is provided by TOF

measurements for low (TOF1) and medium (TOF2) particle momenta. High momentum particles are identified using a Ring Imaging Cherenkov detector (RICH). The BRAHMS PID ability is summarized in Table 1.

Table 1

Upper range of the momentum for 2σ separation (in GeV/c)

	$0 < \eta < 1.0$			$1.5 < \eta < 4.0$		
	TOFW	TOFW2	C4	TOF1	TOF2	RICH
K/π	2.0	2.5	-	3.0	4.5	25.0
K/p	3.5	4.0	9.0	5.5	7.5	35.0

3. OVERALL BULK CHARACTERISTICS

The multiplicity distribution of emitted particles is a fundamental observable in ultra-relativistic collisions. It is sensitive to all stages of the reaction and can address issues such as the role of hard scatterings between partons and the interaction of these partons in the high-density medium [18–20]. Figure 1 shows the measured pseudo-rapidity density of charged hadrons, $dN_{ch}/d\eta$, over a wide range of η for central (0–5%) Au+Au collisions at $\sqrt{s_{NN}} = 200$ GeV, 130 GeV and 62.4 GeV. For central collisions at $\sqrt{s_{NN}} = 200$ GeV we observe about 4500 charged particles within the rapidity range covered by the detection system and $dN_{ch}/d\eta|_{\eta=0} = 625 \pm 56$. The latter value exceeds the particle production per participant pair observed in elementary p+p collisions at the same energy by 40 - 50% [21]. This means that nucleus-nucleus collisions at the considered energies are far from being the simple superposition of elementary nucleon-nucleon collisions.

The measurement of charged particle density $dN_{ch}/d\eta$ can be used to estimate the so-called Bjorken energy density, ε [22]. The formula

$$\varepsilon = \frac{3}{2} \times \frac{\langle E_t \rangle}{\pi R^2 \tau_o} \times \frac{dN_{ch}}{d\eta} \quad (1)$$

provides the value of about 4 GeV/fm³. To obtain this result we assumed that $\tau_o = 1$ fm/c, $\langle E_t \rangle = 0.5$ GeV and $R = 6$ fm. The factor 3/2 is due to the assumption that the charged particles carry out of the reaction zone only a fraction (2/3) of the total available energy. The more refined results obtained from identified particle abundances and particle spectra leads to somewhat larger values of ε , namely 5 GeV/fm³ at $\sqrt{s_{NN}} = 200$ GeV, 4.4 GeV/fm³ at $\sqrt{s_{NN}} = 130$ GeV, and 3.7 GeV/fm³ at $\sqrt{s_{NN}} = 62.4$ GeV, [23]. All of these values significantly exceed the predicted energy density $\varepsilon \approx 1$ GeV/fm³ for the boundary between hadronic and partonic phases of nuclear matter [24].

3.1. Hadrochemistry with BRAHMS data

BRAHMS measures anti-particle to particle ratios for pions, N_{π^-}/N_{π^+} , kaons, N_{K^-}/N_{K^+} , and protons, $N_{\bar{p}}/N_p$, over a large rapidity interval. The results, for Au+Au collision at $\sqrt{s_{NN}} = 200$ GeV and $\sqrt{s_{NN}} = 62.4$ GeV are presented in Figure 2. Whereas N_{π^-}/N_{π^+}

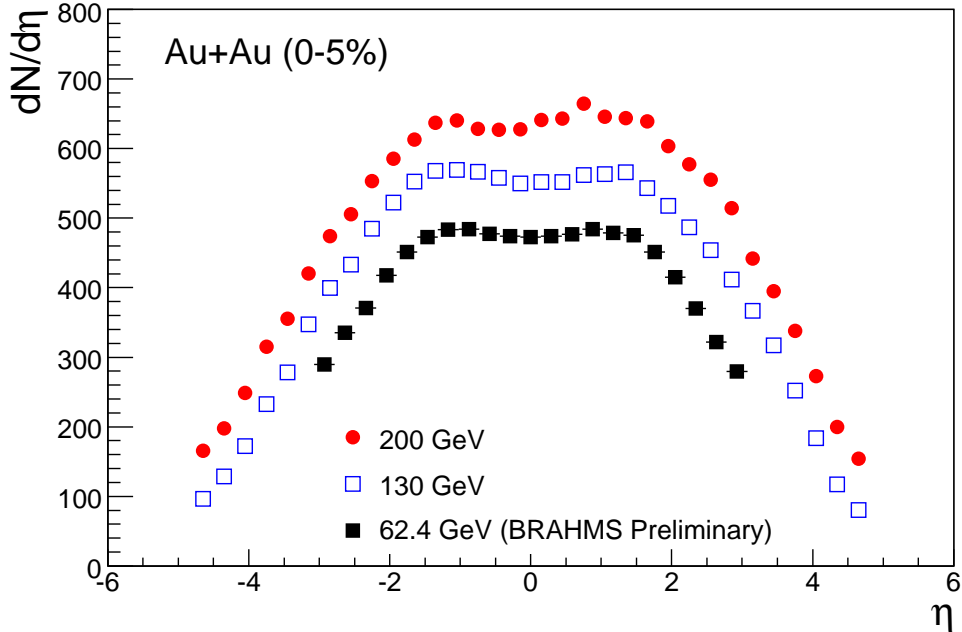


Figure 1. Distributions of $dN_{ch}/d\eta$ measured by BRAHMS for 0 – 5% central Au+Au reactions, at $\sqrt{s_{NN}} = 200$ GeV (solid circles), $\sqrt{s_{NN}} = 130$ GeV (open squares) and $\sqrt{s_{NN}} = 62.4$ GeV (solid squares). Only statistical errors (usually smaller than the symbol size) are shown.

stays constant and is equal to 1 over the covered rapidity range ($0 < y < 3.2$) for both energies, the N_{K^-}/N_{K^+} and $N_{\bar{p}}/N_p$ ratios drop significantly with increasing rapidity. For $\sqrt{s_{NN}} = 200$ GeV the N_{K^-}/N_{K^+} and $N_{\bar{p}}/N_p$ ratios are equal, respectively to 0.95 and 0.76 at $y \approx 0$, and reach values of 0.6 for N_{K^-}/N_{K^+} and 0.3 for $N_{\bar{p}}/N_p$ around rapidity 3. Comparing $\sqrt{s_{NN}} = 200$ GeV and $\sqrt{s_{NN}} = 62.4$ GeV we observe a 11% and 40% decrease of the ratio at mid-rapidity and a 43% and 93% decrease at $y \approx 3$ for kaons and protons, respectively. The large change in the $N_{\bar{p}}/N_p$ ratio from $\sqrt{s_{NN}} = 200$ GeV to $\sqrt{s_{NN}} = 62.4$ GeV is due to the fact that the rapidity $y \approx 3$ for the lower energy corresponding to the fragmentation region, whereas for $\sqrt{s_{NN}} = 200$ GeV, $y \approx 3$ is located about 1 unit of rapidity below the maximum in the net-baryon distribution [25].

Figure 3 shows the N_{K^-}/N_{K^+} ratio as a function of the corresponding $N_{\bar{p}}/N_p$ for various rapidities. The presented results were obtained for central collisions at three RHIC collision energies. The AGS and SPS results are plotted for comparison. There is a striking correlation between the RHIC/BRAHMS kaon and proton ratios over 3 units of rapidity. It is worth noting that the BRAHMS forward rapidity data measured at $\sqrt{s_{NN}} = 62.4$ GeV overlap with the SPS points that were measured at much lower energy but at mid-rapidity. The solid line in Figure 3 shows a fit with a statistical model to the $\sqrt{s_{NN}} = 200$ GeV results, only, assuming that the temperature at the chemical freeze-out is 170 MeV [26,27]. It is seen that the data are very well described by the statistical model over a broad rapidity range with the baryon chemical potential changing from 27 MeV at

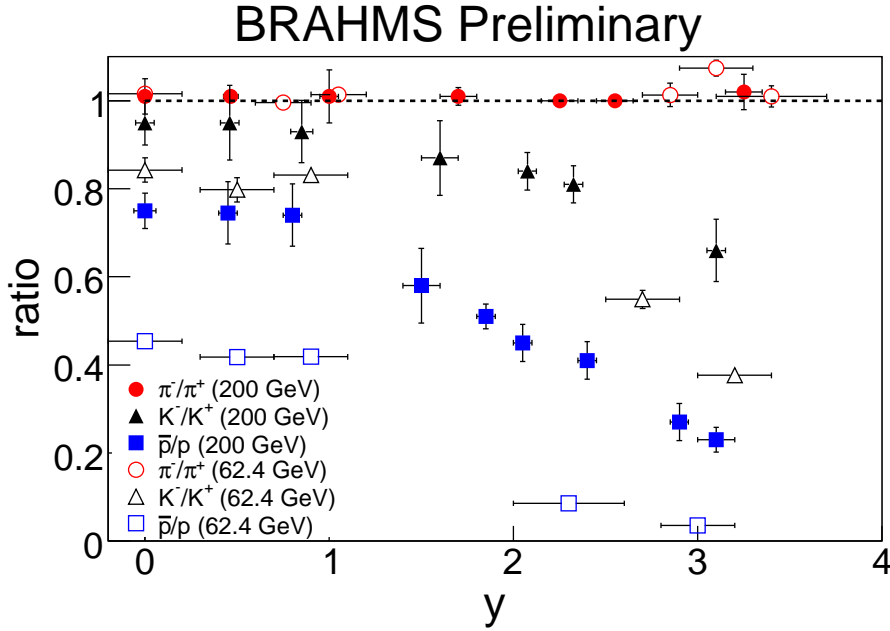


Figure 2. Ratios of anti-particles to particles (pions, kaons and protons) as a function of rapidity for $\sqrt{s_{NN}} = 62.4$ GeV, $\sqrt{s_{NN}} = 200$ GeV. Statistical and systematic errors are indicated.

mid-rapidity to 140 MeV at the most forward rapidities. Using simple statistical models at the quark level with chemical and thermal equilibrium, the ratios can be written as

$$\frac{N_{\bar{p}}}{N_p} = e^{-6\mu_{u,d}/T}, \quad \frac{N_{K^-}}{N_{K^+}} = e^{-2(\mu_{u,d}-\mu_s)/T}, \quad (2)$$

where μ and T are the chemical potential and temperature, respectively. Substituting $\mu_s = 0$ into eqs. (2), one gets $N_{K^-}/N_{K^+} = [N_{\bar{p}}/N_p]^{1/3}$. This relation, represented by the dotted line on Figure 3, does not reproduce the observed correlation. The data are, however, well fitted by the function $N_{K^-}/N_{K^+} = [N_{\bar{p}}/N_p]^{1/4}$ (dashed line) which can be derived from eqs. (2) assuming $\mu_s = 1/4\mu_{u,d}$.

Recently, STAR and NA49 have measured mid-rapidity ratios $\bar{\Lambda}/\Lambda$, $\bar{\Xi}/\Xi$ and $\bar{\Omega}/\Omega$ versus $N_{\bar{p}}/N_p$ for a set of energies from $\sqrt{s_{NN}} = 10$ GeV up to $\sqrt{s_{NN}} = 200$ GeV. These preliminary results can also be well described within a statistical model of chemical and thermal equilibrium at the quark level and confirm the strong correlation between μ_s and $\mu_{u,d}$ derived from BRAHMS data.

3.2. Radial flow

The properties of matter in the latest stage of the collision when the interactions between particles cease (kinetic freeze-out) can be studied from the shapes of emitted particle spectra. These shapes depend in general on the temperature of the emitting source and on the collective flow. For central collisions where one should not expect any azimuthal dependence, only the so-called transverse flow is important [10]. In the blast-wave approach [28] the spectrum is parametrized by a function which depends on the freeze-out temperature, T_{fo} , and on the transverse expansion velocity, β_T . Figure 4 shows results

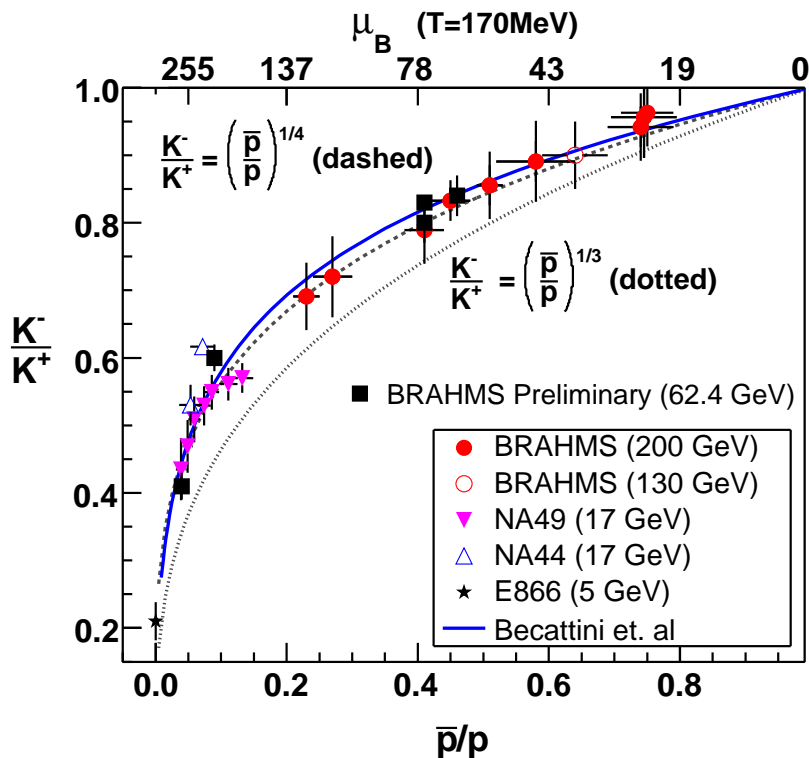


Figure 3. Correlation between N_{K^-}/N_{K^+} and $N_{\bar{p}}/N_p$. The solid curve refer to statistical model calculation with a chemical freeze-out temperature of 170 MeV.

obtained from the analysis of the Au+Au reactions at $\sqrt{s_{NN}} = 200$ GeV. The blast-wave model was used to fit, simultaneously, the π^+ , π^- , K^+ , K^- , protons and anti-protons spectra. The results are plotted versus the number of participants, N_{part} .

One can see that the kinetic freeze-out temperature decreases with centrality from about 140 MeV for the 40 – 50% centrality bin to about 120 MeV for the most central collisions. The latter value is lower than the temperature of chemical freeze-out indicating that, as expected, the freeze-out of particle ratios occurs earlier than the kinetic freeze-out. The reversed trend is seen for the expansion velocity which is equal to about 0.65c and 0.75c for 40 – 50% and 0 – 5% collision centrality, respectively. For comparison we show also the result for the central Au+Au collisions at $\sqrt{s_{NN}} = 62.4$ GeV. Although for the same value of N_{part} the T_{fo} value for both energies is very similar, a reduction by about 20% in the expansion velocity is observed.

Figure 5 shows the dependence of T_{fo} and β_T as a function of rapidity. The observed variations of T_{fo} and β_T on N_{part} and rapidity are consistent with the hydrodynamic description in which the radial flow is the result of outwards gradients of pressure that exist in the expanding matter during the whole evolution. Thus the speed of expansion should increase with the density of the initially created system. The transverse expansion velocity is larger than that observed at SPS energies, which is consistent with a large initial density of the system created at RHIC.

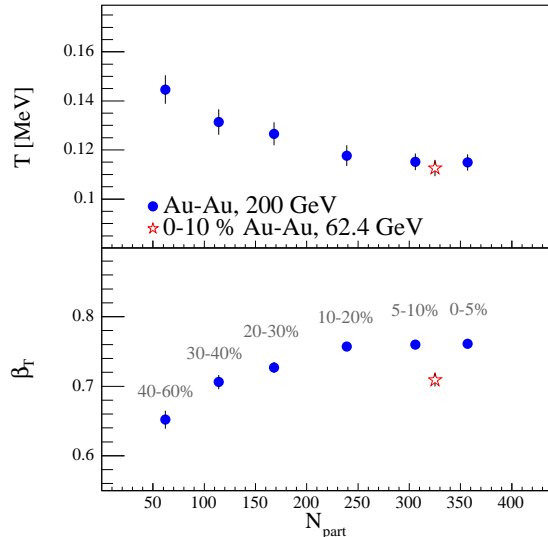


Figure 4. Kinetic freeze-out temperature and transverse flow velocity at mid-rapidity as a function of centrality for Au+Au at $\sqrt{s_{NN}} = 200$ GeV (dots). For comparison we show the result for 0 – 10% central Au+Au collisions at $\sqrt{s_{NN}} = 62.4$ GeV (stars).

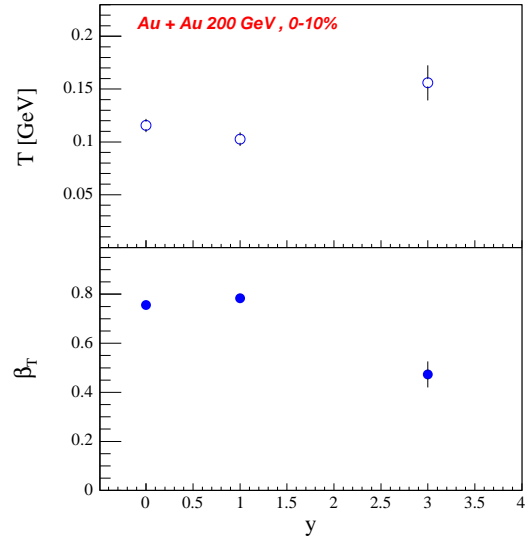


Figure 5. Kinetic freeze-out temperature and transverse flow velocity for central Au+Au collisions at $\sqrt{s_{NN}} = 200$ GeV as a function of rapidity.

3.3. Elliptic Flow

A powerful tool for studying the dynamics that drive the initial evolution of systems created in heavy ion reactions is the analysis of the azimuthal distribution of the emitted particles relative to the reaction plane [10]. The triple differential distribution of emitted particles can be factorized as follows

$$\frac{dN}{dydp_Td\phi} = \frac{dN}{dydp_T} \frac{1}{2\pi} \times (1 + 2v_1(y, p_T)\cos(\phi - \phi_r) + 2v_2(y, p_T)\cos 2(\phi - \phi_r) + \dots), \quad (3)$$

where ϕ and ϕ_r denote the azimuthal angles of the particle and of the reaction plane, respectively. The first factor depends only on y and p_T and the second factor represents the expansion of the azimuthal dependence into a Fourier series. The coefficients of the first (v_1) and the second (v_2) harmonics are called direct and elliptic flow parameters, respectively, and in general they are functions of rapidity and transverse momentum. Calculations based on hydrodynamic models [10] show that elliptic flow is substantially generated only during the highest density phase, before the initial spatial anisotropy of the created medium disappears. Thus v_2 is sensitive to the very early phase in the system evolution and relatively insensitive to the late stage characterized by the dissipative expansion of the hadronic gas.

Elliptic flow has been extensively measured by the STAR, PHENIX and PHOBOS experiments [7–9]. Generally, v_2 is an increasing function of p_T up to 1.5 GeV/c, at which

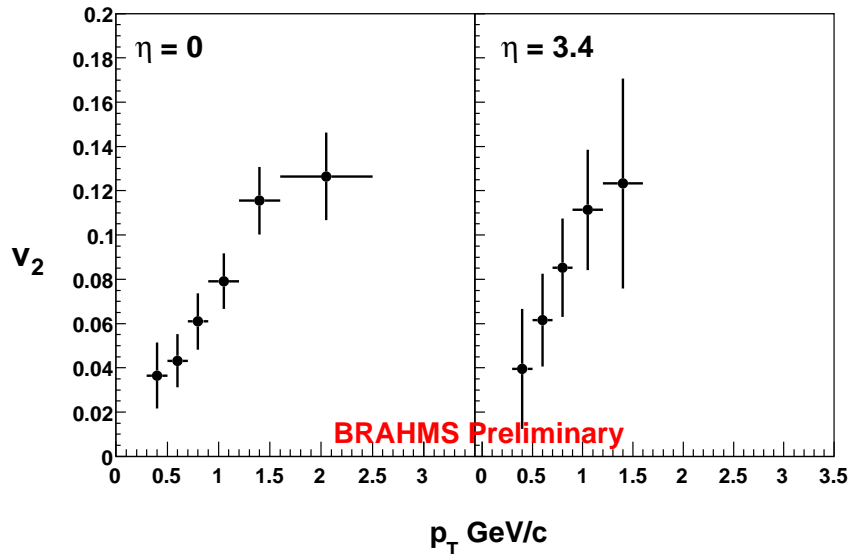


Figure 6. Pion elliptic flow parameter p_T dependence measured for Au+Au at $\sqrt{s_{NN}} = 200$ GeV at $\eta = 0$ and at $\eta = 3.4$.

point it saturates. Up to roughly 1.5 GeV/c in p_T , hydrodynamic calculations show good agreement with experimental data for the v_2 dependence on p_T and centrality.

BRAHMS has measured the p_T dependence of v_2 at a number of rapidities [29], and the results for pions at $\eta = 0$ and at $\eta = 3.4$ are shown in Fig. 6. The elliptic flow parameter, v_2 , for identified pions is an increasing function of p_T at both rapidities. The dependence on pseudo-rapidity is very small. These results are very similar to those obtained for charged hadrons [29].

4. BARYON TO MESON RATIOS

With its excellent particle identification capabilities, BRAHMS can study the p_T and y dependence of hadron production. Preliminary results [30,31] indicate that for Au+Au reactions in the intermediate p_T region the proton to meson ratio is significantly higher than one would expect from the parton fragmentation in vacuum process. Several theoretical models have been proposed to explain the observed enhancement. These range from models that explore the partonic interactions of quark hadronization and quark coalescence [32–34] to models that incorporate novel baryon dynamics [35,36]. The recent experimental data obtained for the p+p, Au+Au, and Cu+Cu colliding systems are expected to result in a better understanding of the underlying physics. Fig. 7 shows a recent investigation by BRAHMS [37] of the \bar{p}/π^- ratios at mid-rapidity (circles) and at pseudo-rapidity $\eta \approx 3.2$ (squares) for Au+Au collisions at $\sqrt{s_{NN}} = 200$ GeV for the different centrality classes indicated on the plot. The data reveal a smooth increase of \bar{p}/π^- ratios from peripheral to central collisions, however, the centrality dependence is stronger at mid-rapidity than at forward rapidity. The maxima in the \bar{p}/π^- ratios are lower at forward rapidity as compared to mid-rapidity. Figure 8 shows the \bar{p}/π^- centrality de-

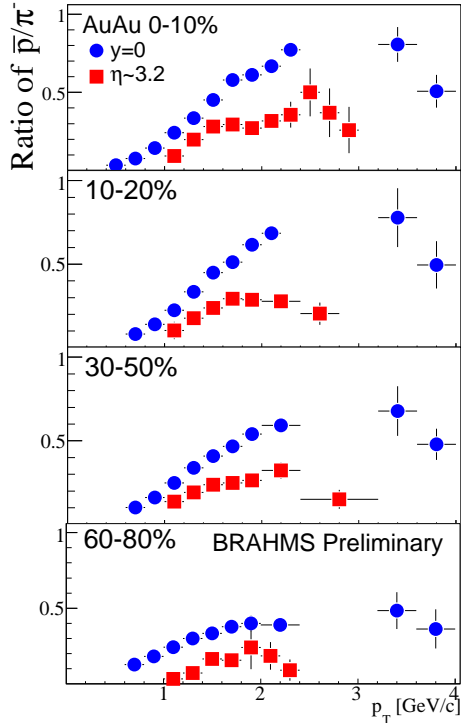


Figure 7. The \bar{p} to π^- ratios at mid-rapidity (circles) and at pseudorapidity $\eta \approx 3.2$ (squares) for different centralities of Au+Au collisions at $\sqrt{s_{NN}} = 200$ GeV.

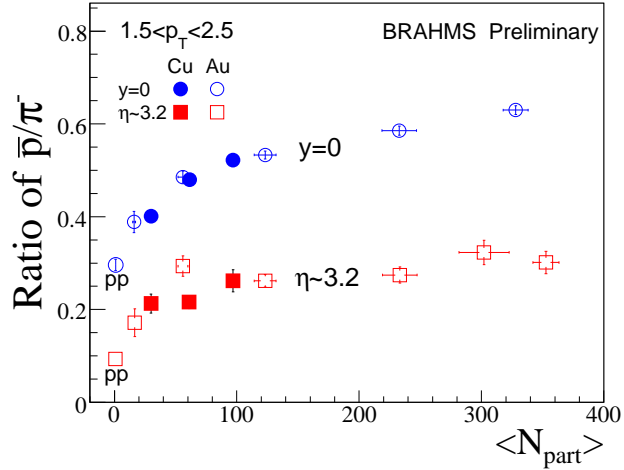


Figure 8. The averaged \bar{p}/π^- versus $\langle N_{part} \rangle$ for Au+Au (open symbols) and Cu+Cu (solid symbols) at $\sqrt{s_{NN}} = 200$ GeV, for $y \approx 0$ (circles) and for $\eta \approx 3.2$ (squares).

pendence for Au+Au (open symbols) and Cu+Cu (solid symbols) at $\sqrt{s_{NN}} = 200$ GeV. The data for $y = 0$ and $\eta \approx 3.2$ are represented by circles and squares, respectively. One can see the strong increase of the \bar{p}/π^- ratios as a function of N_{part} in the range $0 < N_{part} < 60$. For $N_{part} > 60$ the dependence starts to saturate and the ratios reach values of about 0.6 and about 0.25 for central collisions at mid- and forward rapidities, respectively. For peripheral Au+Au collisions the data approach the p+p results. It is important to note that the Au+Au and Cu+Cu ratios are consistent with each other when plotted versus $\langle N_{part} \rangle$, indicating that the \bar{p}/π^- ratio is controlled by the initial size of the created systems. Fig. 9 shows the comparison of BRAHMS and PHENIX data for the ratio of protons to positive pions measured at $y = 0$. The parton coalescence [33] and recombination [34] models describe the observed ratios well at mid-rapidity, as shown in the figure by the dashed curve. The three-dimensional hydrodynamic model [38] (solid curve) cannot reproduce the observed shape of the p/π^+ ratio, however it reproduces the overall level of enhancement. The current hydrodynamic calculations do not show a rapidity dependence which is contrary to the experimental observation (see Fig. 9). This is presumably because the hydrodynamic models assume a rapidity-independent potential.

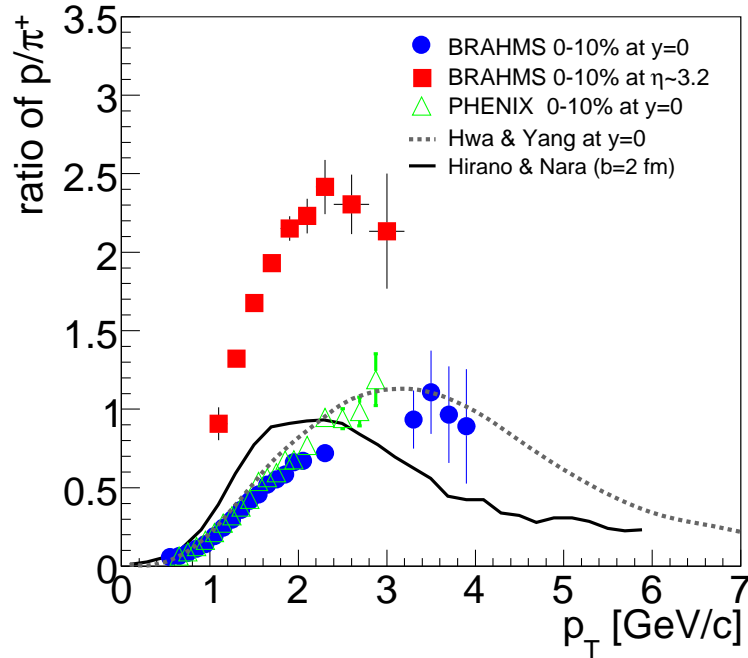


Figure 9. The p/π^+ ratio versus p_T for Au+Au collisions at $\sqrt{s_{NN}} = 200$ GeV measured at mid-rapidity by BRAHMS (circles) and by PHENIX (triangles). Squares represent BRAHMS results at $\eta \approx 3.2$. The plotted lines show model calculations (see text).

5. HIGH p_T SUPPRESSION

Particles with high p_T (above 2 GeV/c) are primarily produced in hard scattering processes early in the collision. In high energy nucleon-nucleon reactions hard scattered partons fragment into jets of hadrons. However, in nucleus-nucleus collisions hard scattered partons might travel in the medium. It was predicted that if the medium is a QGP, the partons will lose a large fraction of their energy by induced gluon radiation, effectively suppressing the jet production [39]. Experimentally this phenomenon, known as jet quenching, will be observed as a depletion of the high p_T region in hadron spectra.

The measure most commonly used to study the medium effects is called the nuclear modification factor, R_{AA} . It is defined as the ratio of the particle yield produced in nucleus-nucleus collision, scaled with the number of binary collisions (N_{coll}), and the particle yield produced in elementary nucleon-nucleon collisions:

$$R_{AA} = \frac{Yield(AA)}{N_{coll} \times Yield(NN)}. \quad (4)$$

At high p_T the particles are predominantly produced by hard scatterings and in the absence of nuclear effects (when the nucleus-nucleus collision reduces to the superposition of elementary collisions) we expect R_{AA} to be 1. At low p_T , where the production rate scales rather with N_{part} , R_{AA} should converge to N_{part}/N_{coll} which is roughly 1/3 for central Au+Au collisions at the top RHIC energy. $R_{AA} < 1$ at high p_T will indicate the suppression which, as has been discussed, can be attributed to the jet quenching

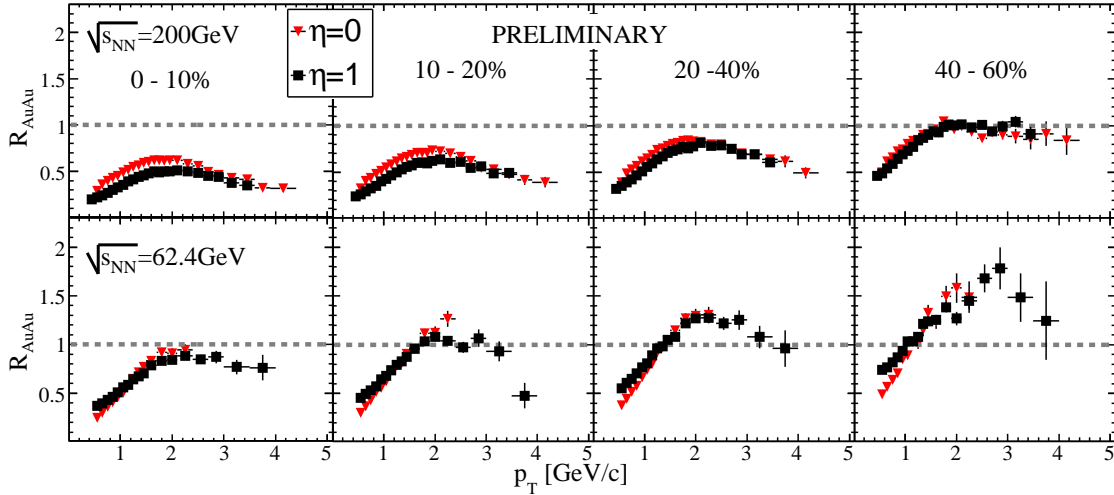


Figure 10. R_{AA} for charged hadrons measured at $\eta = 0$ and $\eta = 1$ for Au+Au at $\sqrt{s_{NN}} = 200$ GeV (upper row) and at $\sqrt{s_{NN}} = 62.4$ GeV (bottom row), for different centrality bins indicated on the plot (p+p reference for $\sqrt{s_{NN}} = 62.4$ GeV is based on ISR collider data [40]).

phenomenon. At SPS there is no suppression. In fact it is well known that there is enhancement for $p_T > 2$ GeV/c. This so-called Cronin effect is attributed to initial multiple scattering of reacting partons.

Another variable used to quantify nuclear effects, one that does not depend on the elementary reference spectra, is R_{CP} , defined as the ratio of R_{AA} for central nucleus-nucleus collisions to R_{AA} for peripheral collisions. The idea of using R_{CP} is based on the expectation that any nuclear modification in peripheral collisions will be insignificant. We will show that the latter statement is not true for $R_{CP} = R_{AuAu}(0-10\%)/R_{AuAu}(40-60\%)$.

5.1. R_{AA} evolution on collision centrality and collision energy for Au+Au and Cu+Cu systems (charged hadrons)

The large set of data collected during the RHIC Run-4 and Run-5 has allowed us to carry out the study of the R_{AA} evolution on collision centrality and collision energy for two colliding systems, namely Au+Au and Cu+Cu [41]. Figure 10 shows R_{AA} measured at $\eta = 0$ and $\eta = 1$ for charged hadrons produced in Au+Au reactions at $\sqrt{s_{NN}} = 200$ GeV (upper row) and at $\sqrt{s_{NN}} = 62.4$ GeV (bottom row), for different collision centralities indicated on the plot. For the most central reactions R_{AA} shows suppression for both energies, however, the suppression is significantly stronger at the higher energy. We observe a smooth increase of R_{AA} towards less central collisions, for $\sqrt{s_{NN}} = 200$ GeV, resulting in approximate scaling with N_{coll} for $p_T > 2$ GeV/c for the 40–50% centrality bin. However, at $\sqrt{s_{NN}} = 62.4$ GeV, $R_{AA} \approx 1$ for more central collisions, and a Cronin peak is clearly visible already for the 20–40% centrality class, where R_{AA} reaches value of about 1.3 in the p_T range between 2.0 and 3.0 GeV/c. These observations at $\sqrt{s_{NN}} = 62.4$ GeV are qualitatively consistent with a picture in which there are two competing mechanisms that influence the nuclear modification in the intermediate and high p_T range, namely: jet quenching that dominates at central collisions and Cronin type enhancement (k_T broad-

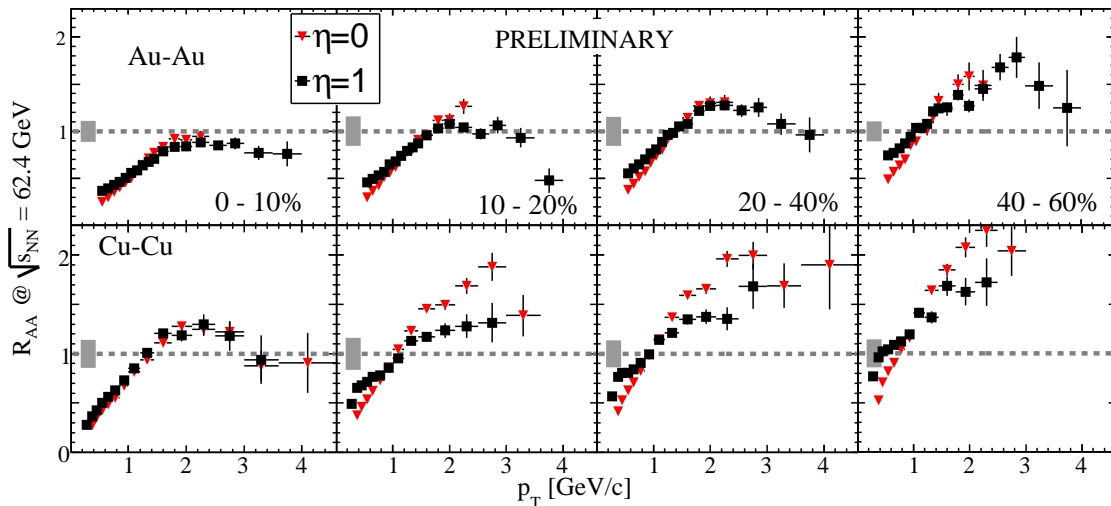


Figure 11. R_{AA} for charged hadrons measured at mid-rapidity for Au+Au (upper row) and for Cu+Cu (bottom row) at $\sqrt{s_{NN}} = 62.4$ GeV for different centrality ranges indicated on the plot.

ening or/and quark recombination) that prevails for the more peripheral collisions.

Figure 11 presents similar comparison as shown on Fig. 10 but this time we compare two different systems, namely Au+Au and Cu+Cu colliding at the same energy ($\sqrt{s_{NN}} = 62.4$ GeV). For Cu+Cu at $\sqrt{s_{NN}} = 62.4$ GeV the same trend of increasing R_{AA} with decreasing collision centrality is seen. However, now the Cronin type enhancement is present already for the most central collisions.

Summarizing the whole set of observations we conclude that the level of suppression of the inclusive hadron spectra produced in nucleus-nucleus collisions at RHIC energies in the p_T range above 2 GeV/c increases with increasing collision energy, collision centrality and with the size of the colliding nuclei. The dependency on the last two variables can be replaced by only one dependency on N_{part} [41].

5.2. R_{AA} for identified hadrons at forward rapidity for Au+Au at $\sqrt{s_{NN}} = 200$ GeV

The BRAHMS collaboration has already noted that the nuclear modification factor in central Au+Au at $\sqrt{s_{NN}} = 200$ GeV at $\eta = 2.2$ is comparable to that measured at mid-rapidity [11] for the same system and energy. However, the data did not clearly identify the mechanism responsible for the observed effect. In this section we present more exclusive analysis of nuclear effects at forward rapidity for identified pions, kaons and protons.

Figure 12 shows R_{AA} for identified hadrons at rapidity $y \approx 3.2$ for 0 – 10% central Au+Au events at $\sqrt{s_{NN}} = 200$ GeV. The shaded band around unity indicates the systematic error associated with the uncertainty in the number of binary collisions. Both R_{AA} and R_{CP} show suppression for pions (left panel) and for kaons (middle panel), however for protons (right panel) R_{CP} shows suppression whereas R_{AA} reveals a Cronin type enhancement with the peak at $p_T \approx 2$ GeV/c. The difference between R_{AA} and R_{CP} for protons is striking, indicating significant enhancement of protons (with respect to p+p)

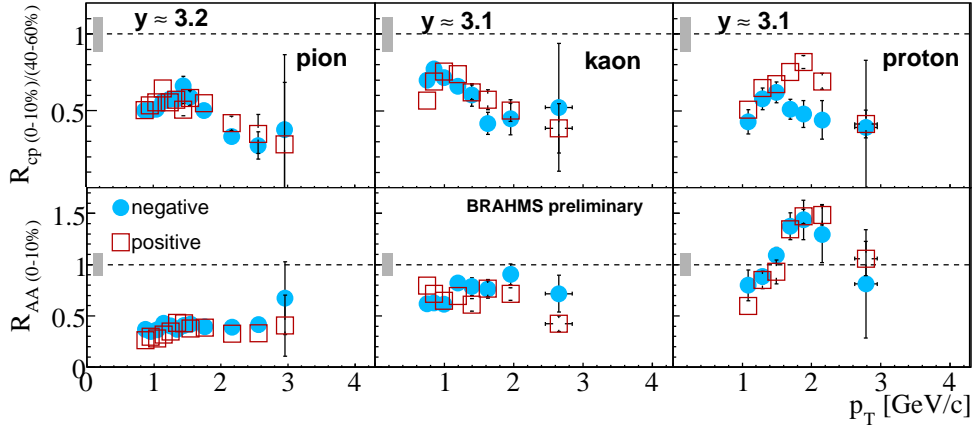


Figure 12. BRAHMS R_{AA} (upper row) and R_{CP} (bottom row) for pions, kaons and protons, measured $y \approx 3.2$ in Au+Au $\sqrt{s_{NN}} = 200$ GeV. The p+p reference was also measured by BRAHMS (see [42]).

for the 40 – 60% collision centrality used in the definition of R_{CP} . The same misleading behavior of R_{CP} is seen for charged hadrons when comparing evolution of R_{AA} and R_{CP} on η for Au+Au at $\sqrt{s_{NN}} = 200$ GeV and $\sqrt{s_{NN}} = 62.4$ GeV [41].

Figure 13 shows the nuclear modification factors found for $(\pi^+ + \pi^-)/2$ (left panel) and $(p + \bar{p})/2$ (right panel), respectively, at $y \approx 3.2$, for central Au+Au reaction. For the comparison we also show the R_{AA} values measured by the PHENIX Collaboration at mid-rapidity. The R_{AA} measured for pions shows strong suppression (by factor of

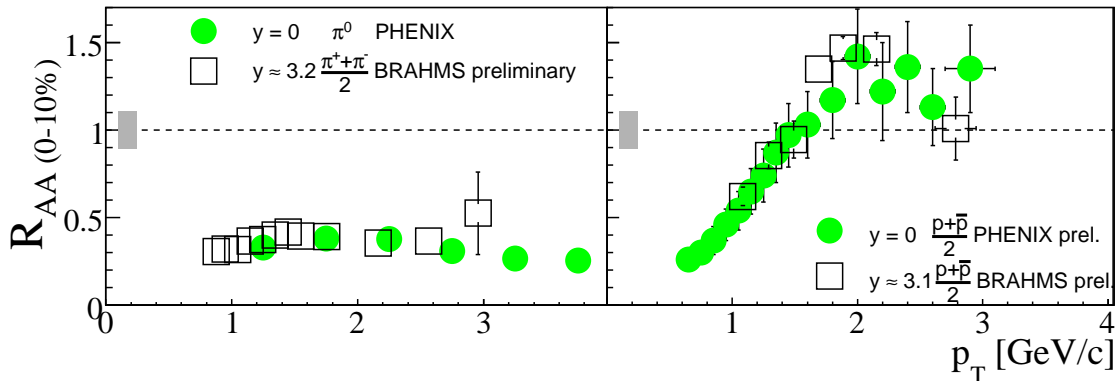


Figure 13. Comparison of R_{AA} measured for central Au+Au collisions at $\sqrt{s_{NN}} = 200$ GeV, at mid-rapidity and $y \approx 3$ for pions (left panel) and protons (right panel).

about 3 for $2 < p_T < 3$ GeV/c), both at mid- and at forward rapidity. The consistency between mid- and forward rapidity is seen also for protons, but in this case, R_{AA} reveals a Cronin peak around $p_T = 2$ GeV/c. The similarity between R_{AA} at mid- and forward rapidity observed simultaneously for pions and protons suggests the same mechanisms is responsible for the nuclear modifications within the studied rapidity interval.

It has been predicted [43] that the magnitude of jet quenching should depend on both the size and the density of the created absorbing medium, thus it is interesting to study the dependence of R_{AA} on centrality. In Figure 14 we plot the averaged R_{AA} measured for pions versus $\langle N_{part} \rangle$ for mid-rapidity (solid circles) and for forward rapidity (open squares). The averaging was performed in the p_T range from 2 GeV/c to 3 GeV/c. Once again, the mid- and forward rapidity pion suppression for the most central Au+Au

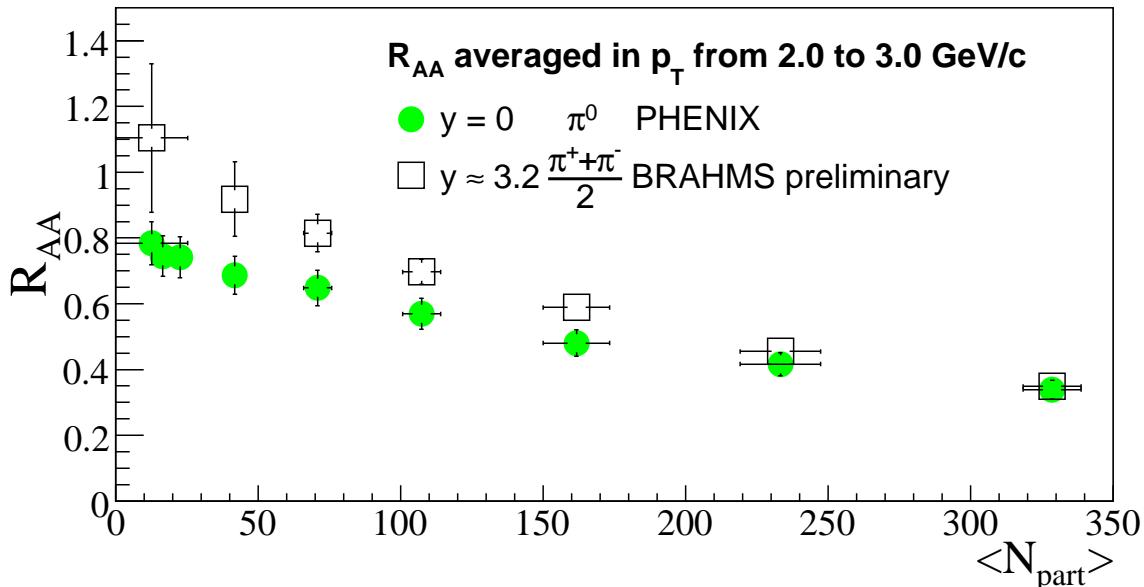


Figure 14. Averaged R_{AA} in the range $2.0 < p_T < 3.0$ GeV/c at mid-rapidity (PHENIX) and at forward rapidity as a function of collision centrality, expressed by the number of participants.

reaction are found of the same strength. However, the R_{AA} measured at forward rapidity shows significantly stronger rise towards peripheral collisions as compared to R_{AA} at mid-rapidity, differing on the level of 35% for $\langle N_{part} \rangle \approx 100$. The trend is consistent with the model of parton energy loss in a strongly absorbing medium [44,45]. In this picture, for $y = 0$, the jet emission is dominated by the emission from the surface which quenches the dependence of R_{AA} on the system size. On the other hand, for $y \approx 3$, the transition from surface to volume emission can occur, which leads to a stronger dependence on N_{part} .

6. SUMMARY

The results from BRAHMS and the other RHIC experiments clearly show that studies of high energy nucleus-nucleus collisions have moved to a qualitatively new physics domain. The collisions are characterized by a high degree of reaction transparency leading to the formation of a near-baryon-free central region with approximate balance between matter and antimatter. From the measurement of charged particle multiplicities in this region lower limits for the energy density at $\tau_o = 1$ fm/c have been determined as 5 GeV/fm³ and 3.7 GeV/fm³, for central Au+Au reactions at $\sqrt{s_{NN}} = 200$ GeV and $\sqrt{s_{NN}} = 62.4$ GeV,

respectively. Therefore the conditions necessary for the formation of a deconfined system appear to be well fulfilled at RHIC energies. Analysis within the statistical model of the relative abundances of K^- , K^+ , p and \bar{p} suggests equilibrium at a chemical freeze-out temperature of 170 MeV, with a noticeably strong correlation between the strange quark and baryon chemical potentials. Analysis of particle spectra within the blast-wave model indicates a kinetic freeze-out temperature on the order of 120 MeV and a large transverse expansion velocity, which is consistent with the high initial energy density.

The measurement of the elliptic flow parameter v_2 versus rapidity and p_T shows weak dependence of the p_T differential v_2 on rapidity. The p/π ratios were measured within $0 < \eta < 3$ for Au+Au and Cu+Cu at $\sqrt{s_{NN}} = 200$ GeV and $\sqrt{s_{NN}} = 62.4$ GeV. The obtained results reveal strong enhancement of baryon to meson ratios in nucleus-nucleus collisions as compare to p+p collisions. Models that incorporate an interplay between soft and hard processes can describe the data at mid-rapidity. We compared R_{AA} for Au+Au at $\sqrt{s_{NN}} = 200$ GeV and $\sqrt{s_{NN}} = 62.4$ GeV, and for Au+Au and Cu+Cu at $\sqrt{s_{NN}} = 200$ GeV. The general observed trend is that R_{AA} increases with: decreasing collision energy, decreasing system size, and when going towards the more peripheral collisions. For Au+Au central collisions at $\sqrt{s_{NN}} = 200$ GeV, R_{AA} shows very weak dependence on rapidity (in $0 < y < 3.2$ interval), both for pions and protons.

REFERENCES

1. E. V. Shuryak, Phys. Lett. B 78 (1978) 150.
2. J. C. Collins and P. J. Perry, Phys. Rev. Lett. 34 (1975) 1353.
3. BRAHMS experimental home pages: <http://www4.rcf.bnl.gov/brahms/WWW/>
4. PHENIX experimental home pages: <http://www.phenix.bnl.gov/>
5. PHOBOS experimental home pages: <http://www.phobos.bnl.gov/>
6. STAR experimental home pages: <http://www.star.bnl.gov/>
7. C. Adler *et al.* [STAR Collaboration], Phys. Rev. C 66 (2002) 034904. J. Adams *et al.* [STAR Collaboration], Phys. Rev. Lett. 92 (2004) 062301.
8. S. S. Adler *et al.* [PHENIX Collaboration], Phys. Rev. Lett. 91 (2003) 182301.
9. B. B. Back *et al.* [PHOBOS Collaboration], nucl-exp/0407012 (2004).
10. P. F. Kolb and U. Heinz, nucl-th/0305084, and references therein.
11. I. Arsene *et al.* [BRAHMS Collaboration], Phys. Rev. Lett. 91 (2003) 072305.
12. D. Kharzeev, Y. V. Kovchegov, and K. Tuchin Phys. Lett. B 599 (2004) 23, and references therein.
13. C. Adler *et al.* [STAR Collaboration], Phys. Rev. Lett. 90 (2003) 082302.
14. C. Adler *et al.* [STAR Collaboration], Nucl. Phys. A 715 (2003) 272.
15. I. Arsene *et al.* [BRAHMS Collaboration], Phys. Rev. Lett. 93 (2004) 242303.
16. J. Jalilia-Marian, Nucl. Phys. A 748 (2005) 664.
17. M. Adamczyk *et al.* [BRAHMS Collaboration], Nucl. Instr. and Meth. A 499 (2003) 437.
18. D. Kharzeev and E. Levin, Phys. Lett. B 599 (2001) 79.
19. I. G. Bearden *et al.* [BRAHMS Collaboration], Phys. Lett. B 523 (2001) 227.
20. I. G. Bearden *et al.* [BRAHMS Collaboration], Phys. Rev. Lett. 88 (2002) 202301.
21. G. J. Alner *et al.*, Z. Phys. C 33 (1986) 1.

22. J. D. Bjorken, Phys. Rev. D 27 (1983) 140.
23. I. G. Bearden *et al.* [BRAHMS Collaboration], Phys. Rev. Lett. 94 (2005) 162301.
24. F. Karsch, Nucl. Phys. A 698 (2002) 199.
25. I. G. Bearden *et al.* [BRAHMS Collaboration], Phys. Rev. Lett. 93 (2004) 102301.
26. I. G. Bearden *et al.* [BRAHMS Collaboration], Phys. Rev. Lett. 90 (2003) 102301.
27. F. Becattini *et al.*, Phys. Rev. C 64 (2001) 024901.
28. P. J. Siemens and J. O. Rasmussen, Phys. Rev. Lett. 42 (1979) 808.
29. H. Ito [BRAHMS Collaboration], “these proceedings”.
30. C. E. Jørgensen *et al.* [BRAHMS Collaboration], Nucl. Phys. A 715 (2003) 741c.
31. Z. Yin *et al.* [BRAHMS Collaboration], J. Phys. G 30 (2004) S983.
32. R. J. Fries *et al.* Phys. Rev. C 68 (2003) 044902.
33. V. Greco, C. M. Ko, and I. Vitev, *et al.* Phys. Rev. C 71 (2005) 041901R.
34. R. C. Hwa and C. B. Yang, Phys. Rev. C 70 (2004) 024905.
35. I. Vitev and M. Gyulassy, Nucl. Phys. A 715 (2003) 779c.
36. V. T. Pop *et al.*, Phys. Rev. C 70 (2004) 064906.
37. Eun Joo Kim [BRAHMS Collaboration], “these proceedings”.
38. T. Hirano, and Y. Nara Phys. Rev. C 68 (2003) 064902
39. X. N. Wang, Phys. Rev. C 58 (1998) 2321.
40. B. Alper *et al.*, Nucl. Phys. B 100 (1975) 237.
41. T. M. Larsen [BRAHMS Collaboration], “these proceedings”.
42. R. Karabowicz [BRAHMS Collaboration], “these proceedings”.
43. M. Gyulassy, P. Levai, and I. Vitev, Nucl. Phys. B 594 (2001) 371. M. Gyulassy, P. Levai, and I. Vitev, Phys. Rev. D 66 (2002) 014005.
44. A. Dainese, C. Loizides, and G. Paić, Eur. Phys. J. C 38 (2005) 461.
45. A. Drees, H. Feng, J. Jia, Phys. Rev. C 71 (2005) 034909.